Theory of the Earth

Don L. Anderson

Chapter 16. Phase Changes and Mantle Mineralogy

Boston: Blackwell Scientific Publications, c1989

Recommended citation:

Anderson, Don L. Theory of the Earth. Boston: Blackwell Scientific Publications, 1989. http://resolver.caltech.edu/CaltechBOOK:1989.001

A scanned image of the entire book may be found at the following persistent URL:

http://resolver.caltech.edu/CaltechBook:1989.001

Abstract:

The densities and seismic velocities of rocks are relatively weak functions of temperature, pressure and composition unless these are accompanied by a drastic change in mineralogy. The physical properties of a rock depend on the proportions and compositions of the various phases or minerals-the mineralogy. These, in turn, depend on temperature, pressure and composition. In general, one cannot assume that the mineralogy is constant as one varies temperature and pressure. Lateral and radial variations of physical properties in the Earth are primarily due to changes in mineralogy. To interpret seismic velocities and density variations requires information about both the stable phase assemblages and the physical properties of minerals.

16

Phase Changes and Mantle Mineralogy

It is my opinion that the Earth is very noble and admirable . . . and if it had contained an immense globe of crystal, wherein nothing had ever changed, I should have esteemed it a wretched lump of no benefit to the Universe.

—GALILEO

The densities and seismic velocities of rocks are relatively weak functions of temperature, pressure and composition unless these are accompanied by a drastic change in mineralogy. The physical properties of a rock depend on the proportions and compositions of the various phases or minerals—the mineralogy. These, in turn, depend on temperature, pressure and composition. In general, one cannot assume that the mineralogy is constant as one varies temperature and pressure. Lateral and radial varia-, tions of physical properties in the Earth are primarily due to changes in mineralogy. To interpret seismic velocities and density variations requires information about both the stable phase assemblages and the physical properties of minerals.

SPHERICAL IONS AND CRUSTAL STRUCTURE

It is often useful to think of a crystal as a packing of different size spheres, the small spheres occupying interstices in a framework of larger ones. In ionic crystals each ion can be treated as a ball with certain radius and charge (Table 16-1). The arrangement of these balls, the crystal structure, follows certain simple rules. The crystal must contain ions in such a ratio so that the crystal is electrically neutral. Maximum stability is associated with regular arrangements that place as many cations around anions as possible, and vice versa, without putting ions with similar charge closer together than their radii allow while bringing cations and anions as close together as possible. In other words, we pack the balls together as closely as possible considering their size and charge. Many crystals are based on cubic close packing or hexagonal close packing of the larger ions.

It is a simple matter of geometry to calculate the ratio of the radii of two types of spheres, **A** and B, that permits a certain number of B to fit around A, and vice versa. If A is very small compared to B, taken as the anion, only two B ions can be arranged to touch A, and the coordination number is 2. When A reaches a critical size, three touching B ions can surround it in a trigonal-planar group, the only regular threefold coordinated structure. The limiting value of the radius ratio for this packing is

$$R_A/R_B = 0.155$$

As A grows still further we reach the point where A can be surrounded by four B as in the SiO_4^{4-} tetrahedron, the basis for many silicates. The R_A/R_B range for this arrangement is 0.225–0.414. For R_A/R_B between 0.414 and 0.732, A can be surrounded by four B in a square planar arrangement or six B in an octahedron arrangement. Rocksalt structures such as NaCl and MgO exhibit octahedral coordination, a common substructural element in silicates. Low-pressure minerals commonly have silicon in tetrahedral coordination and the metals (such as Mg, Fe, Ca, Al) in octahedral coordination. High-pressure phases, such as SiO_2-stishovite, $MgSiO_3$-ilmenite and perovskite, have silicon in octahedral coordination. The mineral majorite,

$$^{VI}Mg_3\ ^{VI}[MgSi]\ ^{IV}Si_3O_{12}$$

has the silicons split between octahedral and tetrahedral sites.

When R_A is almost the size of R_B (R_A/R_B = 0.732–1.0), the cation (A) can be surrounded by eight anions (B) as in a square bipyramid. The anions are at the corners of a

TABLE 16-1
Ionic Radii for Major Mineral-Forming Elements (A)

Ion	*Coordination Number*	*Ionic Radius*	*Ion*	*Coordination Number*	*Ionic Radius*
Al^{3+}	IV	0.39	Fe^{3+}	IV	0.49(HS)*
	V	0.48		VI	0.55(LS)
	VI	0.53		VI	0.65(HS)
Ca^{2+}	VI	1.00	Mg^{2+}	IV	0.49
	VII	1.07		VI	0.72
	VIII	1.12		VIII	0.89
	IX	1.18	Fe^{2+}	IV	0.63(HS)
	X	1.28		VI	0.61(LS)
	XII	1.35		VI	0.77(HS)
Si^{4+}	IV	0.26	Ti^{4+}	V	0.53
	VI	0.40		VI	0.61
Na^{+}	VI	1.02	K^{+}	VI	1.38
	VIII	1.16		VIII	1.51
O^{2-}	II	1.35	F^{-}	II	1.29
	III	1.36		III	1.30
	IV	1.38		IV	1.31
	VI	1.40		VI	1.33
	VIII	1.42	Cl^{-}	VI	1.81

*HS, high spin; LS, low spin.

cube, and the cation is in the center of the cube. CsCl structures fall in this category. The garnet structure has eight M^{2+} ions about each oxygen.

If $R_A = R_B$, twelve B ions can surround each A ion in close packing. The ions can be arranged in two ways, hexagonal close packing or cubic close packing, but the coordination number is 12 in either case. The ideal perovskite structure exhibits twelvefold coordination of the M^{2+} ions around the oxygen ions.

When A and B have the same charge, the anion and cation coordinations are the same because of the requirement of charge neutrality. For AB, compounds neutrality necessitates that the coordination numbers not be the same.

Higher coordination makes for denser packing, and when ionic crystals are compressed, structures with greater coordination numbers tend to form. Common crustal and upper-mantle minerals, however, have such an open packing structure that rearrangements (phase changes) not involving coordination changes usually occur, leading to a more efficient packing of ions, before the coordination-changing transformations can take place. High temperature tends to decrease the coordination.

In the context of rigid spherical ions, the increase of coordination with pressure means that R_A/R_B must increase, necessitating a decrease of R_B, say the oxygen ion, or an increase in R_A. The A–B distance increases as the coordination increases, since more A ions must fit around the B ion, and this is usually assigned to an increase in the cat-ionic radius. The increase in density is due to the decrease in B–B distances from closer packing of the oxygen ions. The increase of A–B and the decrease in B–B means that the attractive potential is decreased and the repulsive, or overlap, potential is increased. This leads to an increase in the bulk modulus or incompressibility.

To a first approximation, then, ionic crystal structures, such as oxides and silicates, consist of relatively large ions, usually the oxygens, in a closest-pack arrangement with the smaller ions filling some of the interstices. The large ions arrange themselves so that the cations do not "rattle" in the interstices. The "nonrattle" requirement of tangency between ions is another way of saying that ions pack so as to minimize the potential energy of the crystal.

In addition to geometric rules of sphere packing and overall charge neutrality, there are additional rules governing ionic crystals that have been codified by Linus Pauling. The considerations discussed so far are equivalent to Pauling's first rule. The second rule states that an ionic structure will be stable to the extent that the sum of the strengths of the electrostatic bonds that reach an anion from adjacent cations equals the charge on the anion. This is the *electrostatic valence principle* or condition of *local* charge neutrality. In general, in a stable ionic crystal the charge on any cation is neutralized by adjacent anions. Cations with large charges must therefore have high coordination numbers and tend to occur in the large interstices or holes in the structure. On the other hand highly charged ions are usu-

small in radius and thus, on the basis of radius ratio, seek to occupy the small holes. Which tendency wins depends on other rules.

Pauling's third rule states that the sharing of edges and particularly of faces by two anion polyhedra decreases the stability of the crystal structure. By this rule, highly charged cations prefer to maintain as large a separation as possible and to have anions intervening between them so as to screen them from each other. This deceases a crystal's potential energy by minimizing the replusive forces existing between nearby cations. Multivalent cations tend to avoid the face-sharing anion cubes of the CsCl structure and prefer the edge-sharing NaCl structure.

The fourth rule, an extension of the third, states that in crystal structures containing different cations, those of high valency and small coordination number tend not to share polyedron elements with each other.

The fifth rule states that the number of essentially different kinds of constituents in a crystal tends to be small; that is, the number of types of interstitial sites in a periodically regular packing of anions tends to be small.

These considerations can be used to understand the stability of crystal lattices. For example, magnesiowiistite, (Mg,Fe)O, is a 6-coordinated phase, making this a low-pressure structure. Packing is relatively inefficient, having a very large volume per oxygen ion relative to other mantle minerals. However *(Mg,Fe)O* is stable to extremely high pressure, probably through most of the lower mantle. The radius ratio of MgO is 0.51, putting it well within the range (0.41–0.73) of expected octahedral coordination. The CsCl structure, with 8-coordination, is displayed by many alkali halides and is the high-pressure form of others that normally display the rocksalt structure. The packing of eight cations around an anion occurs for R_A/R_B greater than 0.732. CsCl itself, for example, has a ratio of 0.93, although at high temperature it adopts the NaCl structure. Likewise RbCl, radius ratio of 0.81, crystallizes in the NaCl structure at low pressure and CsCl at high pressure, being close to the boundary of the radius ratio for these structures. If MgO were to adopt the CsCl structure, the O^{2-} ions would be in contact at the cube faces and the Mg^{2+} ions would be unshielded across cube faces. Each cube would share a face with six others. This makes the CsCl structure unattractive to multicharged ions, such as Mg^{2+}, and pressure apparently is unable to force MgO to bring its ions into closer proximity to achieve a closer packing. The radius ratio $^{VIII}Mg/O$ is 0.63, still outside the range for a CsCl structure. In the NiAs structure, another alternative AB structure, the octahedra share faces, whereas in the NaCl structure they share only edges. Consequently, the *NiAs* structure is not favored by ionic crystals. Thus, MgO has little option but to remain in the rocksalt structure, in spite of the relatively open structure.

Garnet is another mantle mineral that is stable over a large pressure range. The garnet structure consists of independent SiO_4 and AlO_6 polyhedra, which share corners to form a framework within which each M^{2+} ion is surrounded by an irregular polyhedron (a distorted cube) of eight oxygen atoms. In $Mg_3Al_2Si_3O_{12}$ (pyrope) two edges of the silicon tetrahedron and six edges of the aluminum octahedron are shared with the magnesium cube, leaving four unshared edges in the tetrahedron, six in the octahedron and six in the cube. The high percentage of shared edges leads to a tightly packed arrangement, a high density and an apparently stable lattice. In deference to Pauling, most edges are unshared. The packing of oxygen atoms is so efficient that the volume per oxygen atom (15.7 Å^3) is less than in most other high-pressure silicates except ilmenite (14.6), perovskite (13.5) and stishovite (11.6). The M^{2+}-coordination in garnet is 8, so garnet can be considered a high-pressure phase. Because of its relatively low density, it probably remains in the upper mantle. This is an argument against eclogite subduction into the lower mantle.

The polyhedra in garnet are considerably distorted, giving a wide range of Mg–O (in pyrope) and O–O distances and requiring a large unit cell (eight units of $M_3^{2+}M_2^{3+}(SiO_4)^3$ in a cubic unit cell). This distortion reflects Pauling's admonishment against edge sharing involving highly charged ions. Local charge balance is a factor in the structure of pyrope, $Mg_3Al_2Si_3O_{12}$, and other garnets. Each O^{2-} ion bonds to one Si^{4+}, an $A1^{3+}$ and two Mg^{2+} ions. The total of the electrostatic bonds leading to an O^{2-} equals $+2$. If Mg^{2+} were to occupy the octahedral sites, such local charge balance would be impossible. The elastic properties of silicate garnets are relatively insensitive to the nature of the $^{VIII}M^{2+}$ ion.

The garnet structure is particularly important since [MgSi] and [FeSi] can substitute for $[Al]_2$ at high pressure, giving a majorite-garnet solution that may be a dominant phase in the transition region. The large, high-coordination site in garnet allows the garnet structure to accommodate a wide variety of cations including minor elements and elements that are usually termed incompatible, particularly the heavy rare-earth elements (HREE). The crystallization of garnet from a magma can remove these elements, giving a diagnostic HREE depletion signature to such magmas.

Atoms are particularly close packed in body-centered (bcc) and face-centered cubic (fcc) structures. In a body-centered cubic crystal each atom has eight neighbors, and in a face-centered cubic crystal each has twelve neighbors. The atoms can be more closely packed in the face-centered structure. The distance between neighboring atoms in the body-centered case is $a\sqrt{3}/2$, and in the face-centered case it is $a/\sqrt{2}$ where the volume of the unit cell is $a^3/2$ and $a^3/4$, respectively. Assuming spherical ions with radii equal to half these interatomic distances, the volumes of the spheres are $\sqrt{3}\pi a^3/16$ and $\pi a^3/(12\sqrt{2})$ for bcc and fcc. The fraction of the unit cell occupied by spherical ions is 0.68 (bcc) and 0.742 (fcc). The fcc structure has the spheres packed as closely as possible. A rigid sphere can be sur-

rounded by twelve equally spaced neighbors since in this case each sphere touches all of its neighbors.

There are two ways in which one plane of close-packed spheres can fit snugly on top of a similar plane. One gives the fcc structure, and the other gives hexagonal close pack (hcp) structure. If a is the distance between atoms arranged in a hexagon on a plane and c is the distance to the next plane above or below, the distance to the nearest neighbor out of plane is $(a^2/3 + c^2/4)^{1/2}$. For closest packing this equals a, giving $c/a = 1.633$. The volume of the unit cell is $a^2c\sqrt{3}/2$ so that the volume per atom is $a^2c\sqrt{3}/4$. Departures from the ratio $c/a = 1.633$ represent departures from the closest pack.

In simple cubic packing (scp) an ion sits at each corner of a cube. This is an open structure, and unusual properties might be anticipated compared to close-packed structures. The fluorite structures (CaF_2) and CsCl-structures (CsCl, CsI, TlCl) are based on scp of the anions. Cations are at the center of every cube for CsCl and every other cube for CaF_2, the cations being surrounded in each case by eight anions. When the cations approach the size of the anions, the structure resembles bcc in its overall packing for the CsCl structures.

In the rocksalt or NaCl structure the cations by themselves, or the anions, lie on a face-centered cubic lattice. In NaCl, for example, the sodium ions lie in an fcc lattice and chlorine ions are half-way between the Na ions at the centers of the cube edges and at the center of the cube. The alkali halides and oxides of magnesium, calcium, strontium and barium have the NaCl structure. The CsCl structure is not particularly important in mantle mineralogy.

In the rutile (TiO_2) structure each cation has six anion neighbors, two in the plane above, two in the same plane, and two in the plane below. Each anion has three cation neighbors. Stishovite is a high-pressure form of SiO_2 having the rutile structure. Stishovite also forms by the disproportionation of $2MgSiO_3$ to Mg_2SiO_4(β or y) plus SiO_2(st).

As we go to more complex compounds, we have a large variety of possible crystal structures, but many of the more important ones are based on relatively simple packing of the oxygen ions with the generally smaller cations fitting into the interstices. Some cubic minerals mimic the structures of perovskites ($CaTiO_3$), spinels (Al_2MgO_4) or garnets (such as $Mg_3Al_2Si_3O_{12}$-pyrope).

The perovskite structure, $M^{2+}N^{3+}O_3$, has all the atoms arranged in a cubic lattice with the M^{2+} at the corners, the N^{3+} at the center and the O's at the face centers. Generally, the M^{2+} ions (say Mg^{2+}) and the oxygen ions together constitute a cubic close pack structure. All the interatomic distances are determined in terms of one parameter, the side a of the unit cell. The $M^{2+}-0$, $N^{3+}-0$ and $M^{2+}-M^{3+}$ distances are approximately $a/\sqrt{2}$, $a/2$ and $a\sqrt{3}/2$, respectively. These are also approximately the sum of the appropriate ionic radii. In $MgSiO_3$-perovskite there is a considerable range in the individual distances. Although each magnesium is surrounded by twelve oxygens, the Mg–O distances are not all the same. There is therefore a tendency of the structure to distort and not be exactly cubic. Some perovskites are ferroelectric: The displacements of the ions from the positions that they would have in the cubic structure results in a permanent electric dipole for the crystal. If the M^{2+} ion were the same size as the oxygen ions and precisely fit its twelvefold site, then the line joining the centers of the oxygens would equal twice the sum of the ionic radii or 1.414 times the cube's edge. The cube's edge in turn equals twice the sum of the oxygen and M^{4+} radii. The ideal relationship between radii for ions in the perovskite structure is $R(O) + (M^{2+}) = 1.414\ (R(O) + R(M^{4+})t)$ with $t = 1$ (the tolerance factor). In perovskites t generally lies between 0.8 and 1.0. "High-temperature" superconductors have the perovskite structure, with conducting layers alternating with resistive layers of atoms.

Spinel, Al_2MgO_4, is an example of a large class of important compounds, including ferrites, that have important magnetic properties. There are eight magnesium ions per cube of side a. They occupy the centers of four out of the eight small cubes of side $a/2$ into which the larger cube can be divided. Each of the other four small cubes contains four aluminum ions. There are then 16 aluminum ions in the cube of side a. Each aluminum is surrounded by six oxygens, and each magnesium is attached to only four oxygens, an unusual coordination for magnesium. Not all spinels have these site assignments for atoms of different valencies. In some, half of the trivalent atoms are located in tetrahedral sites, and the other half of the trivalent atoms and the divalent atoms are distributed in the octahedral sites. These are called inverse spinels. Examples of inverse spinels include the ferrites Fe_2MgO_4 and Fe_3O_4. The spinel structure is essentially a cubic close pack (fcc) of oxygen ions with metal cations occupying one-eighth of the tetrahedral sites and one-half of the octahedral sites. γ-Mg_2SiO_4 can be viewed approximately as the substitution of Mg^{2+} and Si^{4+} for $A1^{3+}$ and Mg^{2+}.

Garnets are also cubic minerals, and some have important magnetic and optical properties. For silicate garnets (M^{2+} = Mg, Ca, Fe . . .) the unit cube contains 24 M^{2+} ions, 16 aluminums, 24 silicons and 96 oxygens. The coordinations are (for M^{2+} = Mg)

$$^{VIII}Mg_3\ ^{VI}Al_2\ ^{IV}Si_3O_{12}$$

Many substitutions are possible for all the cations, and garnets in the crust and mantle are important repositories for trace elements, particularly those having ionic radii similar to magnesium, calcium and aluminum. The tetrahedral silicate groups, four oxygens tetrahedrally arranged around a central silicon atom, are independent of each other. Garnet is therefore called an island silicate. The elastic properties of garnets are almost independent of the nature of the M^{2+} ion, in contrast to other silicates.

Hexagonal and trigonal crystals are closely related. Calcite ($CaCO_3$) and corundum (Al_2O_3) are trigonal crystals, and one high-pressure form of $MgSiO_3$ is similar to

ilmenite ($FeTiO_3$), another trigonal crystal. In the calcite structure each M^{2+} atom is bonded to six oxygens, and each oxygen is bonded to one M^{4+} and two M^{2+} atoms. We may think of the calcite structure as a distorted *NaCl* structure. The oblate CO_3 group replaces the spherical chloride ion. Calcite is the main constituent of the metamorphic rock marble, a rock with strongly anisotropic properties because of the alignment of the individual calcite crystals. The strong alignment of calcite and of ice, a hexagonal crystal, in natural masses suggests that $MgSiO_3$-ilmenite will also be strongly aligned in the mantle.

In corundum (Al_2O_3) the oxygens occur on equilateral triangles, similar to calcite, but there is no atom at the center of the triangle, in the same plane. The aluminum atoms are not all in a plane. Each aluminum is surrounded by six oxygens. Cr_2O_3 mixes in all proportions with Al_2O_3, Cr^{3+} and $A1^{3+}$ having similar radii, and the mixture yields the gem ruby with its characteristic red color. It has important optical properties. Al_2O_3 may be important in the lower mantle. It is found in some kimberlites.

In ilmenite ($FeTiO_3$) half the aluminums are replaced by iron, half by titanium. This breaks the symmetry, and ilmenites are expected to be more anisotropic than corundums. The oxygens in corundum and ilmenite structures are in approximate hcp.

Some of the more common low-pressure silicates are also based on simple packing of the oxygen ions. In olivine, for example, the oxygens are in approximate hcp. The transformation to the spinel form results in a slight decrease in the Mg–O distance, a slight increase in the Si–O distance and a decrease in the larger of the O–O near-neighbor distances, resulting in an 8 percent decrease in the volume per oxygen and a change in oxygen packing from approximately hcp to approximately bcc. The coordinations of the ions remain the same. Note that

$$^{VI}Mg_2^{2+}\ ^{IV}Si^{4+}\ O_4\text{-spinel}$$

is not analogous to true spinel

$$^{VI}Al_2^{3+}\ ^{IV}Mg^{2+}\ O_4$$

either in the coordination of magnesium or the valency of the ions in the tetrahedral and octahedral sites. Aluminate spinels have some anomalous elastic properties, presumably related to the IV coordination of the M^{2+} ions, which cannot be assumed to carry over to the silicate spinels. In fact, because of the very small size of the ^{IV}Mg ion it must be treated as a different element than ^{VI}Mg.

In this chapter we use mineral names such as spinel, ilmenite and perovskite to refer to structural analogs in silicates rather than to the minerals themselves. This has become conventional in high-pressure petrology and mineral physics, but it can be confusing to those trained in conventional mineralogy with no exposure to the high-pressure world.

Interatomic Distances in Dense Silicates

The elastic properties of minerals depend on interatomic forces and hence on bond type, bond length and packing. As minerals undergo phase changes, the ions are rearranged, increasing the length of some bonds and decreasing others. The interatomic distances and the average volume per oxygen atom are given in Table 16-2 for many of the crystal structures that occur in the mantle. For a given coordination the cation-anion distances are relatively constant. This, in fact, is the basis for ionic radius estimates. Cation-anion distances increase with coordination, as required by packing considerations. It is clear that the increases of density and bulk modulus, K_S, are controlled by the increase in packing efficiency of the oxygen ions.

TABLE 16-2
Average Interatomic Distances (Angstroms), Volume Per Oxygen Ion (Å^3) and Bulk Modulus (GPa) in Mantle Minerals

Mineral or Structure	Mg–O	Si–0	O–O	V/O^{2-}	K_S
MgO	2.11	—	2.98	18.7	163
Olivine	2.11	1.63	2.66–2.99	18.1	129
Pyroxene	2.09	1.63		17.3	108
β-spinel	2.08	1.65	2.69–2.95	16.8	174
y-spinel	2.06	1.67	2.73–2.91	16.5	184
Ilmenite	2.08	1.80	2.54–2.89	14.6	212
Perovskite	2.06–2.20**	1.75–1.82	2.53–2.71	13.5	262
Stishovite	—	1.78	2.16	11.6	316
Garnet	2.27*	1.64	2.5–2.78	15.7	174
Al_2O_3	†	—	2.52	17.0	254

* Al–O distance in garnet is 1.89.
** 4 shortest distances.
† Al–O distance is 1.91.

Crystals and Magmas

Up to this point I have treated crystals as isolated entities. Most mantle crystals are formed from a melt, and it is instructive to consider them from this point of view. The distribution of ions and the nature of the crystals formed depend on properties of both the melt and the solids. The first silicate crystals to form from a cooling magma usually have the Si^{4+} ions as widely separated as possible, in accordance with Pauling's third rule. Oxygen ions touch at most one Si^{4+} ion. No two tetrahedra drawn about each Si^{4+} share a corner, that is, an oxygen. Crystal structures in which each $[SiO_4]^{4-}$ tetrahedron is isolated from all others are called *island silicates* or *nesosilicates* (from the Greek word for "island") or *orthosilicates.* Olivines and garnets are such structures. Bloss (1971) gives a good summary.

As island silicates crystallize from the melt, the remaining liquid is enriched in Si^{4+}, permitting silicates with higher Si^{4+} to O^{2-} ratios to form. The Si^{4+} ions cannot be so widely spaced, and some of the oxygens touch two Si^{4+} ions. β-spinel has linked SiO_4 tetrahedra and is therefore a double-island or *sorosilicate*. With progressive crystallization the Si/O ratio increases further, and Si^{4+} occurs in so many interstices in the crystals that do form that each tetrahedron shares a corner with two others to form $[SiO_3]^{2-}$ chains as in the pyroxenes, which are single-chain or *metasilicates.* With increased cooling, *double-chain silicates* form with $[Si_4O_{11}]^{6-}$ units and a large number of shared corners. Amphiboles are double-chain silicates. At even lower temperatures the Si^{4+} to O^{2-} ratio is higher still, and the $(OH)^-$ to O^{2-} ratio is also high. *Layer silicates* such as micas and talc form under these conditions.

In some structures, the *framework silicates,* the proportion of Si^{4+} to O^{2-} is so high that all tetrahedra share all their corners. The various crystalline forms of SiO_2—quartz, tridymite, cristobalite—are framework structures that crystallize at low temperature. The feldspars are also framework silicates, but Al^{3+} tetrahedra as well as Si^{4+} tetrahedra are involved, so they can also crystallize early.

Most of the structures discussed above have relatively open structures and are unstable at moderate pressures. They also tend to have low seismic velocities and to be anisotropic. The increased packing efficiency of high-pressure mineral phases makes their description in terms of arrangements of tetrahedra and octahedra less useful than a description in terms of dominant sublattices of close-packed ions with the remaining ions occupying available interstices. Nevertheless, it is likely that most minerals in the mantle have crystallized from magmas at low pressure and have subsequently converted to high-pressure phases. Therefore, it is of interest to know the conditions that initially determine the relative proportions of the various constituents of minerals at low pressure. The trace and minor elements follow similar rules. They tend to replace major ions of similar size and valency, or occupy interstices of appropriate size or, for the very incompatible elements, remain in the melt to the end, coating the major crystals with exotic phases.

MINERALS AND PHASES OF THE MANTLE

As far as physical properties and major elements are concerned, the most important upper mantle minerals are olivine, orthopyroxene, clinopyroxene and aluminum-rich phases such as plagioclase, spinel and garnet. Olivine and orthopyroxene are the most refractory phases and tend to occur together, with only minor amounts of other phases, in peridotites. Clinopyroxene and garnet are the most fusible components and also tend to occur together as major phases in rocks such as eclogites.

All of the above minerals are unstable at high pressure and therefore only occur in the upper part of the mantle. Clinopyroxene, diopside plus jadeite, may be stable to depths as great as 500 km. Olivine transforms successively to β-spinel, a distorted spinel-like structure, near 400 km and to y-spinel, a true cubic spinel, near 500 km. At high pressure it disproportionates to $(Mg,Fe)SiO_3$ in the perovskite structure plus (Mg,Fe)O, magnesiowiistite, which has the rocksalt structure. The FeO component is strongly partitioned into the (Mg,Fe)O phase.

Orthopyroxene, $(Mg,Fe)SiO_3$, transforms to a distorted garnet-like phase, majorite, with an increase in coordination of some of the magnesium and silicon:

$$^{VIII}(Mg,Fe)_3{}^{VI}Mg^{VI}Si^{VI}Si_3O_{12}$$

where the Roman numerals signify the coordination. This can be viewed as a garnet with MgSi replacing the Al,. This is a high-temperature transformation. At low temperature the following transformations occur with pressure:

$$2MgSiO_3(opx) \rightarrow Mg_2SiO_4\ (\beta\text{-sp}) + SiO_2(st)$$

$$\rightarrow Mg_2SiO_4(\gamma\text{-sp}) + SiO_2(st) \rightarrow 2\ MgSiO_3\ (ilmenite)$$

$$\rightarrow 2\ MgSiO_3\ (perovskite)$$

A different sequence occurs for $CaMgSi_2O_6$ (diopside clinopyroxene). The ionic radius of calcium is much greater than aluminum, and this is expected to make the transition pressure to the garnet structure much higher than for orthopyroxene.

In the presence of Al_2O_3, or garnet, the pyroxene garnets form solid solutions with ordinary aluminous garnets, the transition pressure decreasing with Al_3O_3 content.

The mineralogy in the transition region, at normal mantle temperatures, is expected to be β- or y-spinel plus garnet solid solutions. At colder temperatures, as in subduction zones, the mineralogy at the base of the transition region is probably y-spinel plus ilmenite solid solution.

The garnet component of the mantle is stable to very

high pressure, becoming, however, less aluminous and more siliceous as it dissolves the pyroxenes. At low temperature and at pressures equivalent to those in the lower part of the transition region, the garnet as well as the pyroxenes are probably in ilmenite solid solutions.

The ilmenite structure of orthopyroxene can be regarded as a substitution of $^{VI}Mg\ ^{VI}Si$ for $^{VI}Al_2$ in the corundum structure. The transformation of $CaMgSi_2O_6$ clinopyroxene to ilmenite, if it occurs, is probably a higher pressure transition. $CaMgSi_2O_6$ may transform to the perovskite structure without an intervening field of ilmenite:

$$^{VIII}(Ca_{0.5}Mg_{0.5})_3\ ^{VI}(Ca_{0.5}Mg_{0.5})\ ^{VI}Si\ ^{IV}Si_3O_{12}$$

$$(\text{``majorite''}) \rightarrow {}^{VIII\text{-}XII}(Ca_{0.5}Mg_{0.5})_4\ ^{VI}Si_4O_{12}\ \text{(perovskite)}$$

The ionic radii (in angstroms) of some of the ions involved in the above reactions are

^{VI}Al, 0.53	^{VIII}Mg, 0.89	^{VI}Ca, 1.00
^{XII}Ca, 1.35	^{VI}Si, 0.40	$^{VI}[CaSi]$, 0.70
^{VI}Mg, 0.72	^{XII}Mg, 1.07	^{VIII}Ca, 1.12
^{IV}Si, 0.26	$^{VI}[MgSi]$, 0.56	

The ionic radius of $^{VI}[MgSi]$ is similar to ^{VI}Al, and therefore a solid-solution series between garnet and majorite at relatively low pressure is expected. The ionic radius of $^{VI}[CaSi]$ is much greater, and therefore diopside is expected to require higher pressures for its garnet transformation unless only the Mg^{2+} enters the octahedral site. The replacement of Al_2 for $Ca_{0.5}\ Mg_{0.5}Si$ in the perovskite structure is also expected to be difficult, so it is possible that clinopyroxene-garnet disproportionates to calcium-rich perovskite plus Al_2O_3, the excess Al_2O_3 probably combining with $MgSiO_3$ $x\ Al_2O_3$ in the garnet, ilmenite or perovskite structure, depending on pressure. The disparity in ionic radii between $^{VIII\text{-}XI}Ca$, $^{VIII\text{-}XII}Mg$, ^{IV}Si and ^{VI}Al probably means that there will be three separate perovskite phases in the lower mantle: Ca-rich, (Mg, Fe)-rich and Al-rich. The presence of Al_2O_3 decreases the density of perovskite but increases the density of ilmenite and garnet.

Ferrous iron (Fe^{2+}) is expected to readily substitute for Mg^{2+} in all the phases discussed so far. The relative partitioning of Fe^{2+} amongst phases, however, is expected to vary with pressure. Garnet is by the far the most Fe^{2+}-rich phase in the upper mantle, followed by olivine, clinopyroxene and orthopyroxene. As the pyroxenes dissolve in the garnet they dilute the Fe/Mg ratio, and y-spinel may be the most iron-rich phase in the lower part of the transition region. In the lower mantle Fe^{2+} favors (Mg,Fe)O over perovskite. When the Fe^{2+} high spin–low spin transition occurs, somewhere deep in the lower mantle, solid solution between Fe^{2+} and Mg^{2+} is probably no longer possible because of the disparity in ionic radii, and a separate FeO-bearing phase, such as Fe(L.S.)O, is likely. At high pressure this is expected to dissolve extensively in any molten iron that traverses this region on the way to the core, or to be stripped out of any mantle that comes into contact with the core in the course of mantle convection. An Fe-O-poor lower mantle is therefore a distinct possibility. The corollary is an iron-FeO core (see Chapter 4).

As far as we know perovskite and MgO are stable throughout the lower mantle, which is consistent with seismic radial homogeneity of most of the lower mantle. $MgSiO_3$-perovskite is the most abundant mineral in the mantle. The seismic properties of the lower mantle are broadly consistent with (Mg,Fe) SiO_3-perovskite, although other phases may be present, such as (Mg,Fe) O.

In general FeO decreases the pressure of phase transitions in the mantle, including olivine–β-spinel, β–γ-spinel and pyroxene-garnet. Al_2O_3 widens the stability fields of garnet and ilmenite. Ca^{2+} is a large ion and in simple compounds is expected to cause phase transitions at lower pressures than the equivalent Mg^{2+} compound. However, the large size of Ca^{2+} makes it difficult to substitute for $A1^{3+}$ (in the coupled CaSi substitution for Al_2). At high temperature clinopyroxene contains excess Mg^{2+} compared to pure diopside,

$$CaMgSi_2O_6 + xMg_2Si_2O_6 = CaMg_{2x+1}\ Si_2O_6$$

Therefore, orthopyroxene probably reacts out of the mantle at shallower depths than clinopyroxene.

The difficulty of substituting $^{VI}[CaSi]$ for $^{VI}[Al_2]$ suggests the following structural formula for diopside-garnet:

$$^{VIII}Ca_2\ ^{VIII}Mg\ ^{VI}[MgSi]\ ^{IV}Si_3O_{12}$$

This has the virtue of requiring no coordination change for Ca^{2+} in going from the diopside to garnet structure.

PHASE EQUILIBRIA IN MANTLE SYSTEMS

The lateral and radial variations of seismic velocity and density depend, to first order, on the stable mineral assemblages and, to second order, on the variation of the velocities with temperature, pressure and composition. Temperature, pressure and composition dictate the compositions and proportions of the various phases. In order to interpret observed seismic velocity profiles, or to predict the velocities for starting composition, one must know both the expected equilibrium assemblage and the properties of the phases.

To a first approximation, olivine, orthopyroxene, clinopyroxene and an aluminous phase (feldspar, spinel, garnet) are stable in the shallow mantle. β-spinel, majorite, garnet and clinopyroxene are stable in the vicinity of 400 km, near the top of the transition region. y-spinel, majorite or y-spinel plus stishovite, Ca-perovskite, garnet and ilmenite are stable between about 500 and 650 km. Garnet, ilmenite, Mg-perovskite, Ca-perovskite and magnesiowüs-

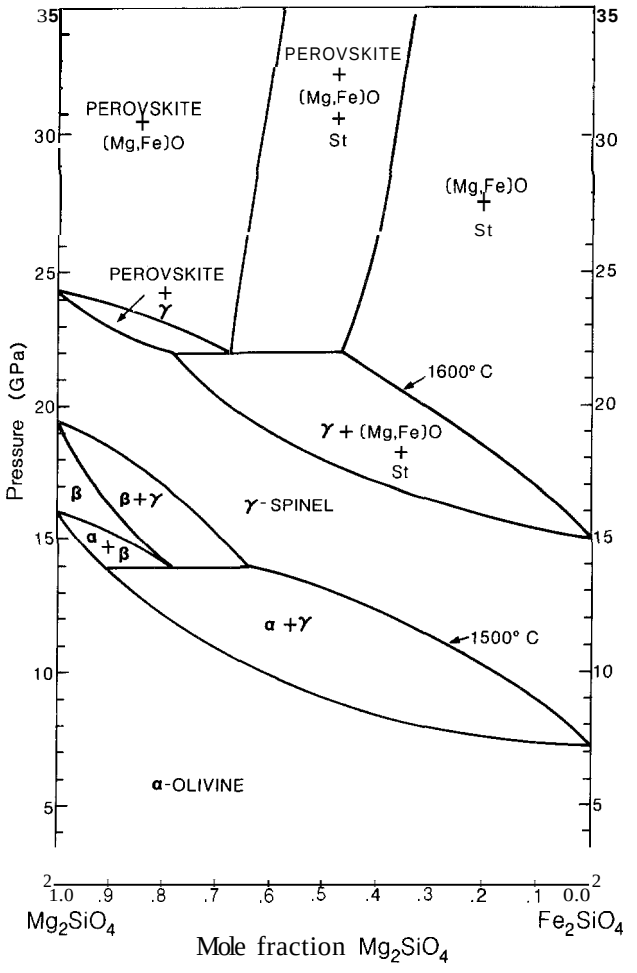

FIGURE 16-1
Phase relations in Mg_2SiO_4–Fe_2SiO_4 system (J. Bass and D. L. Anderson, unpublished).

tite are stable near the top of the upper mantle, and perovskites and magnesiowiistite ± Al_2O_3 are stable throughout most of the lower mantle. The details of the stable assemblages depend on composition and temperature. Lateral variations in velocity due to temperature-induced phase changes can be as important as pressure-induced phase changes are in the radial direction.

Phase equilibria can be discussed in terms of the olivine system, the pyroxene system and the pyroxene-garnet system. Pyroxenes can tolerate a certain amount of Al_2O_3 and garnets, at high pressure, dissolve pyroxene, so pyroxenes and garnets must be treated together. On the other hand the olivine system is almost pure Mg_2SiO_4–Fe_2SiO_4, although FeO can be exchanged with pyroxene-garnet.

Phase equilibria in mantle systems are summarized below in a series of figures based on available experiments and calculations. A useful summary of early work is contained in Ringwood (1975). The olivine system is shown in Figure 16-1.

Pyroxene System

Enstatite (en) and diopside (di) do not form a complete solid-solution series, but en dissolves a certain amount of di, and di contains an appreciable amount of en at moderate temperature and pressure. The amount of mutual solubility increases with temperature and decreases with pressure, and this provides a method for estimating the temperature of equilibration of mantle-derived xenoliths. Pyroxenes also react with garnet:

$$3MgSiO_3 \cdot xAl_2O_3 \rightleftharpoons xMg_3Al_2Si_3O_{12} + 3(1-x)MgSiO_3$$

aluminous enstatite ⇌ garnet + enstatite

which proceeds to the right with increasing pressure (Figure 16-2). In principle, the measurement of the compositions

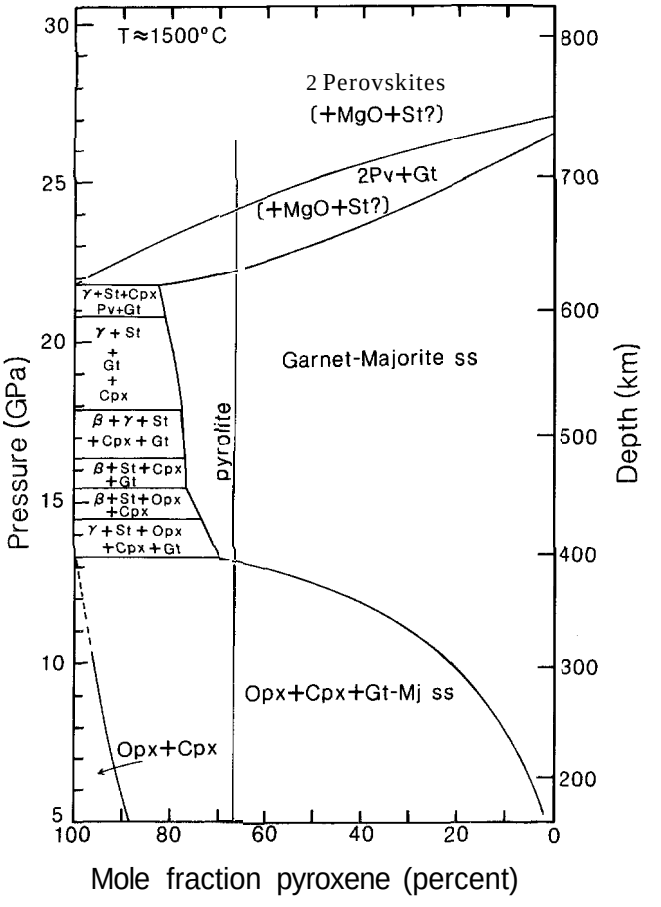

FIGURE 16-2
Phase relations in orthopyroxene-garnet system (J. Bass and D. L. Anderson, unpublished).

of coexisting pyroxenes and garnets provides information about pressures and temperatures in the mantle. At higher pressure garnet dissolves the enstatite, and this requires a change in coordination of one-fourth of the Mg and Si. Pressures in excess of about 100 kbar are required for this change in coordination.

Natural clinopyroxenes, particularly in eclogites, are solid solutions between diopside and jadeite called omphacite:

$$^{VIII}Ca^{VI}Mg^{IV}Si_2O_6 + {}^{VIII}Na^{VI}Al^{IV}Si_2O_6$$

At modest pressure, about 20 kbar, the solid solution series is complete (Figure 16-3). Natural clinopyroxenes from kimberlite eclogites contain up to 8 weight percent Na_2O. Clinopyroxenes from peridotites typically have much less Na_2O and jadeite.

Most garnets contain very little sodium; however, at high pressure Na_2O can enter the garnet lattice (Ringwood, 1975). In particular, the following garnets have been synthesized (Ringwood and Major, 1971):

$$(NaCa_2)\ (AlSi)Si_3O_{12}$$

$$(Na_2Ca)Si_2Si_3O_{12}$$

Natural garnets associated with diamonds in kimberlite pipes contain up to 0.26 percent Na_2O. In the transition region, the sodium is probably contained in a complex garnet solid solution.

The other high-pressure forms of pyroxene include ilmenite, β plus stishovite, γ plus stishovite, ilmenite and perovskite, depending on pressure, temperature and content of calcium, aluminum and iron. The pressures at which clinopyroxene and orthopyroxene disappear are strong functions of the other variables.

The phase behavior of garnet + clinopyroxene + orthopyroxene, the peridotite assemblage, is substantially different from the behavior of garnet + clinopyroxene, the basalt-eclogite assemblage. When only clinopyroxene + garnet are present, the clinopyroxene dissolves in the garnet with increasing pressure and eventually a homogeneous garnet solid solution is formed. When orthopyroxene is also present, the garnet and clinopyroxene compositions move toward orthopyroxene with increasing pressure; that is, the orthopyroxene component dissolves in both the garnet and the clinopyroxene and eventually disappears. At this point an MgSi-rich, aluminum-deficient garnet coexists with a magnesium-rich diopside. Garnet then moves toward the clinopyroxene composition as diopside dissolves in the garnet. Therefore, in contrast to the bimineralic eclogite system, the garnet takes a detour toward MgSiO, before it heads toward $CaMgSi_2O_6$. In either case, orthopyroxene disappears at a relatively low pressure, being either completely absorbed in the garnet structure or partially converting to β + stishovite or γ + stishovite, depending on the garnet, or Al_2O_3, content of the initial mixture. Recent high-pressure, high-temperature experiments have helped elucidate the phase relations in $MgSiO_3$, the main component of the orthopyroxene system. A preliminary synthesis of available results is given in Figure 16-4. Note that the high-temperature sequence of transitions is different from the low-temperature sequence. The resulting densities and seismic velocities are also quite different. The garnet form of MgSiO,, majorite, is dominant at high temperature. Majorite is similar to pyrope garnet with $^{VI}Mg\ ^{VI}Si$ replacing $^{VI}Al_2$ yielding

$$^{VIII}Mg_3\ ^{VI}[MgSi]^{IV}Si_3O_{12}$$

Since $^{VI}[MgSi]O_3$ (periclase plus stishovite) has elastic properties similar to $^{VI}Al_2O_3$, we expect majorite to have elastic properties similar to pyrope.

$^{VI}Mg^{VI}SiO_3$-ilmenite, a high-pressure, low-temperature form of enstatite, has considerable higher elastic moduli since all of the silicon is in sixfold coordination as in stishovite. Ilmenite is extremely anisotropic. The low-

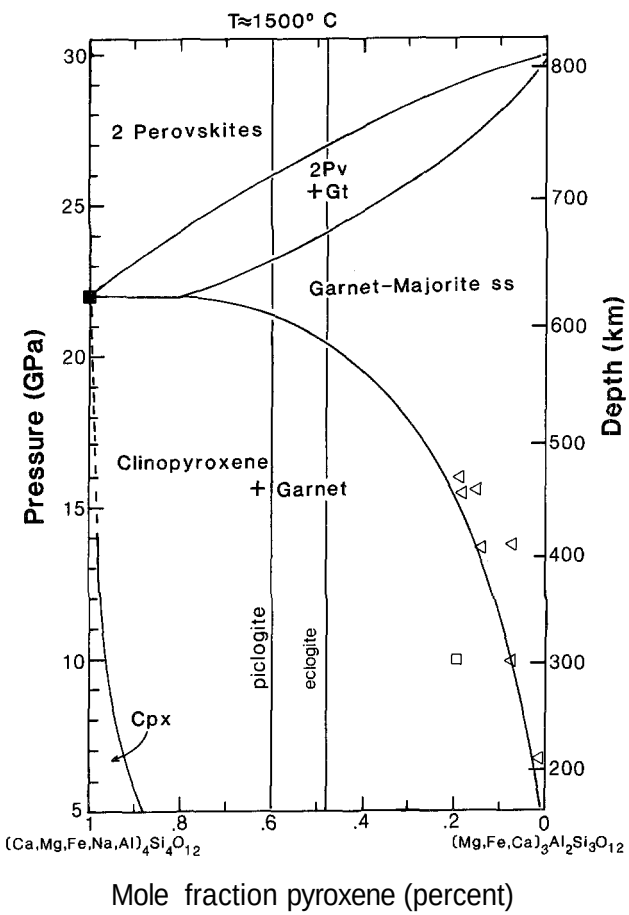

FIGURE 16-3
Phase relations in clinopyroxene-garnet system (J. Bass and D. L. Anderson, unpublished).

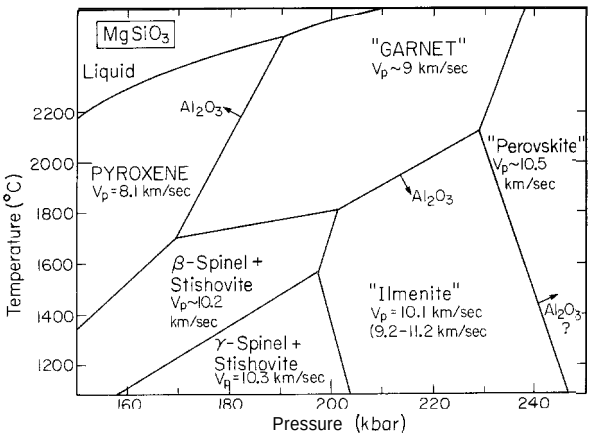

FIGURE 16-4
Provisional phase relations in $MgSiO_3$ (modified from Kato and Kumazawa, 1985, Sawamoto, 1986, and Akaogi and others, 1986). The arrows show the direction that the phase boundaries are expected to move when Al_2O_3, or garnet, is added. The approximate compressional velocities are shown for each phase.

temperature minerals (spinel + stishovite, ilmenite) are 10 percent to 20 percent higher in velocity than the high-temperature minerals (pyroxene, majorite).

The low-temperature assemblages, β + stishovite, γ + stishovite and ilmenite are of the order of 10 percent faster than majorite. The locations of the phase boundaries depend on Al_2O_3 content, and the expected migration direction is given in the figure by the arrows. Note that the garnet form of pyroxene is stabilized by high temperature and high Al_2O_3 content. Also, ordinary pyroxene is stable to relatively high pressures in hot mantle. This is partially responsible for the low velocities in the upper mantle under oceanic and tectonic regions.

The CMAS System

The system $CaO\text{-}MgO\text{-}Al_2O_3\text{-}SiO_2$ (CMAS) is shown in Figure 16-5 in simplified form. The phases of Mg_2SiO_4 are olivine (a), β-spinel (β), y-spinel (y) and perovskite plus MgO (using structural names throughout). The major phases of $MgSiO_3$ are enstatite, majorite, ilmenite and perovskite (Mg-pv). At low temperatures and when little or no Al_2O_3 is present, there are also extensive fields of β + stishovite (st) and γ + stishovite. High temperatures and the presence of Al_2O_3 stabilize the majorite (mj) structure, and a broad majorite-garnet solid-solution field occurs between enstatite, ilmenite and perovskite. Diopside and jadeite, components of clinopyroxene, are stable to higher pressures than enstatite. Diopside collapses to a dense calcium-rich phase, probably perovskite (Ca-pv), at pressures less than required to transform enstatite to perovskite (Ringwood, 1975, 1982). Garnet (gt) itself is stable throughout most of the upper mantle, although it dissolves pyroxene with increasing pressure. At very high pressure, garnet transforms to an Al_2O_3-rich perovskite (Al-pv) (Liu, 1974). The lower mantle below about 750 km probably consists of three perovskites plus magnesiowiistite (3 pv + mw).

Note that the phase assemblages along the "cold slab" adiabat are different from those along the "normal mantle" adiabat at almost all pressures, and this is true also for temperature contrasts much smaller than the 800°C chosen for purposes of illustration. The $\alpha-\beta$ transition is elevated by 30 kbar and the $\beta-\gamma$ transition is elevated by 40 kbar in the cold slab. In the case of enstatite, not only is the upper stability limit decreased at low temperature, but the low-temperature phase assemblages are different. The dense and fast phase y-spinel has a much broader stability field in cold mantle.

Different phase assemblages are also encountered as one increases the temperature from the "normal mantle" adiabat. The partial melt field (not shown) is encountered at

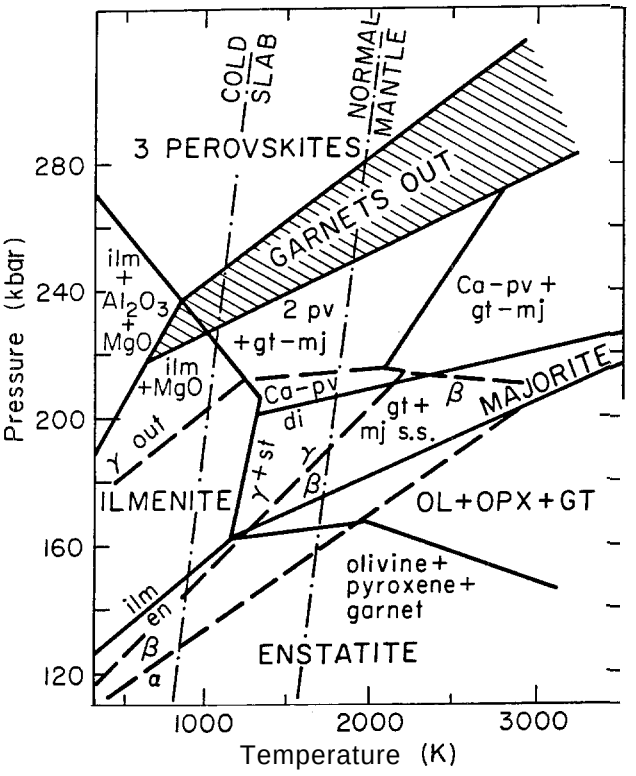

FIGURE 16-5
Equilibrium phase boundaries for mantle minerals modified from Kuskov and Galimzyanov (1985) and Ito and Takahashi (1986). Dashed lines are olivine system boundaries; solid lines are pyroxene-garnet system boundaries. Approximate adiabats are shown for "normal" mantle and "cold slab" mantle. Note the different phase assemblages, at constant pressure, for the two adiabats. Most boundaries are for pure end-members in the system $CaO\text{-}MgO\text{-}Al_2O_3\text{-}SiO_2$.

low pressure. The fields of the low-pressure, low-density assemblages are expanded at high temperature, but the change in density is not symmetric about the average, or normal, temperature. The thermal expansion coefficient increases with temperature, so there is a larger decrease of density for a given increase in temperature than for the corresponding decrease. For an internally heated mantle, upwellings are broader than downwellings, so the lateral changes in physical properties are expected to be more diffuse than for the slab.

The peridotite mineral assemblage, olivine + pyroxenes + garnet, stable in the shallow mantle, has transformed by *190* kbar to β- or y-spinel + majorite + garnet ± clinopyroxene ± stishovite with a substantial increase in density and seismic velocity. This is for a normal mantle adiabat. At this pressure, but at temperatures 400°C colder, this assemblage is replaced by ilmenite, y-spinel and magnesiowiistite ± calcium-rich perovskite. At *230–260* kbar the normal mineral assemblage is two perovskites + garnet, while the cold assemblage is three perovskites or calcium-perovskite + garnet + ilmenite + oxides. By *280* kbar the assemblages should be independent of temperature over the temperature range expected in the lower mantle. Temperature-induced variations in density and velocity should, therefore, be relatively small below *770* km. Note the very broad stability fields of garnet-majorite solid solution in high-temperature mantle and y-spinel and ilmenite in cold mantle. Also note the negative Clapeyron slope for the ilmenite-perovskite transition.

CALCULATION OF PHASE RELATIONS

The standard free energy of a reaction is given by

$$\Delta G^{\circ}(P,T) = \Delta H^{\circ}_{\mathrm{T}} - T\Delta S^{\circ}_{\mathrm{T}} + \int_{1}^{P} \Delta V(P,T)\mathrm{d}P$$

where ΔH°_{T} and ΔS°_{T} are the enthalpy and entropy of reaction, respectively, at temperature T and are given by

$$\Delta H^{\circ}_{\mathrm{T}} = \Delta H^{\circ}_{T_{\mathrm{o}}} + \int_{T_{\mathrm{o}}}^{T} \Delta C_{\mathrm{p}}\, \mathrm{d}T$$

$$\Delta S^{\circ}_{\mathrm{T}} = \Delta S^{\circ}_{T_{\mathrm{o}}} + \int_{\sim}^{T} (\Delta C_{\mathrm{p}}/T)\mathrm{d}T$$

where T_{o} is a standard temperature and AC, is the heat capacity difference between products and reactants. At equilibrium

$$\Delta G^{\circ}(P,T) = 0$$

The slope of the reaction, in P,T space, is given by

$$\mathrm{d}P/\mathrm{d}T = \Delta S/\Delta V$$

Values of AS and AV are given in Table *16-3*.

TABLE 16-3
Thermochemical Data for Phase Transitions

Transition	ΔV°_{298} (cm³/mol)	ΔS°_{1000} (cal/mol K)	ΔS°_{298} (cal/mol K)
Mg_2SiO_4			
$\alpha\rightarrow\beta$	−3.13	−2.5	−3.1
$\beta\rightarrow\gamma$	−0.89	−1.5	−0.9
$\alpha\rightarrow\gamma$	−4.02	−4.0	−4.0
$\beta\rightarrow$ox	−4.03	+1.92	—
$\gamma\rightarrow$ox	−3.14	+3.36	−0.35
$\gamma\rightarrow$pv + *mw*	−3.84	—	−3.2
γ+st→2ilm	−0.79	+2.71	−1.9
β+st→2ilm	−1.89	+0.48	—
$MgSiO_3$			
2px→β+*st*	−7.99	−5.63	−4.95
2px→γ+*st*	−9.09	−7.86	−5.85
px→ilm	−4.94	−2.58	−3.6
ilm→pv	−1.91	—	−2.0
px→pv	−6.83	—	−5.9
px→gt	−2.74	−3.5	—
SiO_2(q)→st	−9.70	−3.24	—

Navrotsky and others (1979), Watanabe (1982), Akaogi and others (1984), Ito and Navrotsky (1985).

ISOBARIC PHASE CHANGES AND LATERAL VARIATIONS OF PHYSICAL PROPERTIES

As the ability to map the three-dimensional structure of the Earth improves, it becomes important to understand the factors that influence the lateral heterogeneity in density and seismic velocities. Much of the radial structure of the Earth is due to changes in mineralogy resulting from pressure-induced equilibrium phase changes or changes in composition. The phase fields depend on temperature as well as pressure so that, for example, a given mineral assemblage will occur at a different depth in colder parts of the mantle. The elevation of the olivine-spinel phase boundary in cold slabs is probably the best known example of this effect. The other important minerals of the mantle, orthopyroxene, clinopyroxene and garnet, also undergo temperature-dependent phase changes to denser phases with higher elastic moduli. These phases include majorite, ilmenite, spinel plus stishovite, and perovskite. The pronounced low-velocity zone under oceans and tectonic regions and its suppression under shields is another example of phase differences (partial melting) associated with lateral temperature gradients.

Temperature provides more than just a perturbation to the depths of phase boundaries. Variations in temperature, at constant pressure, also cause changes in the stable mineral assemblages, and these isobaric phase changes result in larger changes in the physical properties than are caused by the effect of temperature alone. In general, the sequence of phase changes that occurs with increasing pressure also occurs with decreasing temperature. There are also some mineral assemblages that do not exist under normal conditions of pressure and temperature but occur only under the extremes of temperature found in cold slabs or near the solidus in hot upwellings. Generally, the cold assemblages are characterized by high density and high elastic moduli.

The magnitude of the horizontal temperature gradients in the mantle are unknown, but slab modeling suggests about 800°C over about 50 km. In an internally heated material the upwellings are much broader than slabs or downwellings. Tomographic results show extensive low-velocity regions associated with ridges and tectonic regions, consistent with broad high-temperature regions. The cores of convection cells have relatively low thermal gradients. We therefore expect the role of isobaric phase changes to be most important and most concentrated in regions of subducting slabs. The temperature drop across a downwelling is roughly equivalent to a pressure increase of 50 kbar, using typical Clapeyron slopes of upper-mantle phase transitions.

In the recent geophysics literature it is often assumed that lateral variations in density and seismic velocity are due to temperature alone. By contrast, it is well known that radial variations are controlled not only by temperature and pressure but also by pressure-induced phase changes. Phase changes such as partial melting, basalt-eclogite, olivine-spinel-postspinel, and pyroxene-majorite-perovskite dominate the radial variations in density and seismic velocity. It would be futile to attempt to explain the radial variations in the upper mantle, particularly across the 400- and 650-km discontinuities, in terms of temperature and pressure and a constant mineralogy. All of the above phase changes, plus others, also occur as the temperature is changed at constant pressure or depth. Yet it is common practice to ignore these temperature-induced phase changes in attempting to explain geophysical anomalies associated with the geoid and slabs, and the ocean-continent contrast. This has led to models requiring deep slab penetration, since temperature alone is not sufficient to explain the magnitude of the anomalies if slabs are confined to the upper mantle. Likewise, the integrated travel-time contrast between shields and oceans implies a thick continental root unless lateral phase changes, such as partial melting, are allowed for. In any case the large lateral variations in velocity above 300 km, and particularly above 200 km, make it difficult to resolve variations below 400 km, and those that are resolved are small and uncorrelated with shields. Lateral density and velocity variations associated with phase changes are not confined to narrow depth intervals, nor are they all associated with simple elevation of phase boundaries in cold mantle. The combination of cold temperature and high pressure can stabilize assemblages that are not present in warmer mantle and can broaden, in depth, the stability fields of high-density minerals.

There are large geoid and seismic velocity anomalies associated with subducting slabs. Ordinary temperature effects are so small that slab penetration deep into the lower mantle has been invoked in order to explain the size of the anomalies. This, in turn, has been used by some to support models of whole-mantle convection and to reject chemically stratified models with slabs confined to the upper mantle.

Because of lateral temperature gradients we have to be concerned with lateral, or isobaric, phase changes as well as radial phase changes. Some of these phase changes, their approximate depth extent in "normal" mantle and the density contrasts include the following:

50–60 km	basalt → eclogite (15 percent)
50–60 km	spinel peridotite → garnet peridotite (3 percent)
50–200 km	partial melting (10 percent)
400–420 km	olivine → β-spinel (7 percent)
300–400 km	orthopyroxene → majorite (10 percent)
500–580 km	→ β + st(4.5 percent) → y + st(1.6 percent)
500–580 km	β-spinel → y-spinel (3 percent)

400–500 km	clinopyroxene → garnet (10 percent)
500 km	garnet-majorite s.s. → ilmenite s.s. (5 percent)
700 km	ilrnenite → perovskite (5 percent)

For a multicomponent mantle the above percentages must be multiplied by the fraction of mantle involved.

Most of these reactions have positive Clapeyron slopes and are therefore elevated in cold slabs and depressed in hot upwellings. The density contrasts are much larger than those associated with thermal expansion and, in any case, add to the thermal expansion effect. This is important in geoid modeling. The associated velocity contrasts are important in modeling lateral changes in seismic velocity and slab anomalies. For a coefficient of thermal expansion of $3 \times 10^{5}/°C$, it requires a temperature change of $10^{3}°C$ to change the density by 3 percent. Since the thermal coefficients of density and elastic moduli decrease with compression, it is even more difficult to obtain large lateral variations at depth with temperature alone.

SLABS

One result of the neglect of isobaric phase changes is the conclusion that density and velocity anomalies in the upper mantle are not sufficient to explain the magnitude of slab-related geoid and seismic anomalies. Hager (1984) calculated the geoid signal by associating slabs with an average density contrast of 0.1 g/cm^3. This can explain the geoid signal for whole-mantle convection models. When phase changes are included, the average density contrast of slabs is about 3 times greater, being about 0.4 g/cm^3 midway through the upper mantle. In the whole-mantle flow models, this agreement is a result of the large density-geoid kernels associated with whole-mantle convection. In chemically layered models the density-geoid response goes to zero at chemical boundaries, and the average value of the upper-mantle kernel is much less than for the whole-mantle case. Therefore, a large density contrast is consistent with stratified convection.

There are several phase changes in cold subducting material that contribute to the increase in the relative density of the slab. The basalt-eclogite transition is elevated, contributing a 15 percent density increase for the basaltic portion of the slab in the upper 60 km or so. The absence of melt in the slab relative to the surrounding asthenosphere increases the density and velocity anomaly of the slab in the upper 300 km or so of the mantle. The olivine-spinel and pyroxene-majorite phase changes are elevated by some 100 km above the 400-km discontinuity, contributing about 10 percent to the density contrast in the upper mantle. The $\beta-\gamma$ transition is also elevated, adding several percent to the density of the slab between 400 and 500 km. The ilmenite form of pyroxene is 5 percent denser than garnetite, increasing the density contrast of the cold slab between 500 and 670 km, relative to hot mantle, by about a factor of 2 or 3 over that computed from thermal expansion. In addition to these effects, the formation of a detached thermal boundary layer below the 650-km discontinuity can also increase the total mass anomaly associated with subduction. The latter can increase or decrease the geoid anomaly associated with subduction, depending on the nature of the chemical layering (Richards and Hager, 1984).

The seismic anomaly associated with slabs is also much greater than can be accounted for by the effect of temperature on velocity. Phase changes, including partial melting outside the slab, may be the cause. The associated density contrast between slab and normal mantle is greater than between the plate and the underlying mantle as estimated from thermal expansion alone.

The ilmenite form of $MgSiO_3$ is a stable phase, at low temperature, in the lower part of the transition region (Figure 16-4). Ilmenite is about 8 percent denser than garnet-majorite and has a V_p about 10 percent greater. Although ilmenite is only 4 percent slower than perovskite, it is 7 percent less dense. Ilmenite becomes stable at slab temperatures somewhere between 450 and 600 km and is predicted to remain stable to depths greater than the perovskite phase boundary in higher-temperature mantle. Although the slab is predicted to be locally less dense than the lower mantle at about 650 km, it will probably depress the boundary between the upper and lower mantles because of the accumulated density excess and the negative Clapeyron slope between ilmenite-spinel and perovskite-MgO. The $CaMgSi_2O_6$-component of the mantle transforms to perovskite at a slightly lower pressure than the comparable transformation in $MgSiO_3$, and the transformation pressure is lower at low temperature. These all contribute to the velocity and density anomaly of the slab at the base of the transition region.

In the discussion so far we have assumed that the slab is identical in composition to the adjacent mantle. Yet the slab is probably laminated: The upper layer is basalt/eclogite, and the second layer is probably olivine-orthopyroxene harzburgite. These undergo their own series of phase changes and, when cold, remain denser than garnet peridotite to at least 500 km.

The composition of the lower oceanic lithosphere is unknown. The alternatives are basalt-depleted peridotite, or harzburgite, undepleted peridotite and basalt/eclogite. The last could be the result of underplating of the oceanic lithosphere by melts from the mantle. Cold harzburgite averages about 0.1 g/cm^3 denser than warm pyrolite between 400 and 600 km (Ringwood, 1982). At 600 km it becomes less dense. Eclogite is denser than peridotite at the same temperature to depths of 500–560 km (Anderson, 1982; Anderson and Bass, 1986) and, when cold, to 680 km (Irifune and Ringwood, 1986). Cold eclogite is about 4–5 percent

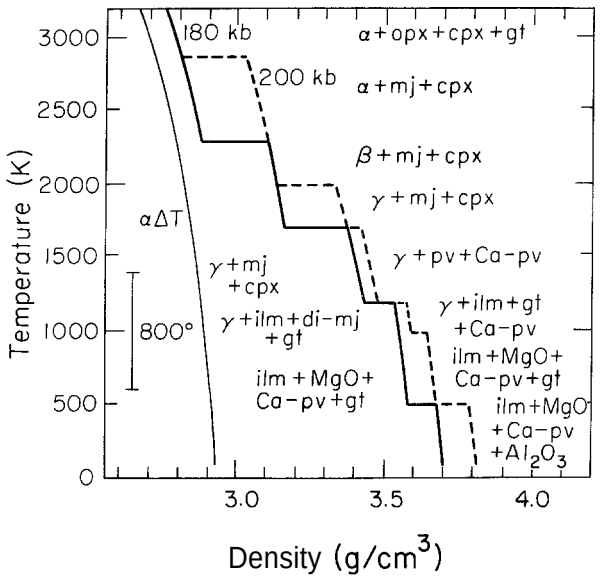

FIGURE 16-6
Approximate variation of zero-pressure density with temperature taking into account thermal expansion (curve to left) and phase changes at two pressures. The effect of pressure on density is not included. $\alpha\Delta T$ is not linear since α increases with T and generally decreases from low-density to high-density phases. The inclusion of density jumps associated with phase changes increases the average effect of temperature by a factor of 3 to 4. At phase boundaries the effect is much larger. The phases stable over each temperature interval are also shown. The abbreviations are α(olivine), β(β-spinel), γ(γ-spinel), opx (orthopyroxene),cpx (clinopyroxene), gt (garnet), mj ($MgSiO_3$-majorite), pv ($MgSiO_3$-perovskite), Ca-pv ($CaSiO_3$-perovskite), ilm ($MgSiO_3$-ilmenite) (after Anderson, 1987b).

denser than warm peridotite above 550 km depth. If the 650-km discontinuity is a chemical boundary, this boundary will be depressed by the integrated density excess in overlying cold mantle even if the deeper part of the slab is buoyant. The "650-km discontinuity" is expected to be an irregular boundary in a chemically stratified mantle and to be much deeper under slabs. In any event it appears that the different phase assemblages in the slab relative to warm mantle will contribute to the density contrast. An increase of intrinsic density between upper and lower mantle and a negative Clapeyron slope will inhibit slab penetration into the lower mantle. Hager (1984) invoked an increase in viscosity at 650 km to partially support the slab in order to explain the geoid highs associated with subduction zones. A chemical change has a similar effect.

The approximate zero-pressure density as a function of temperature, at two pressures, is shown in Figure 16-6. Temperature is plotted increasing upward to emphasize the fact that decreasing temperature has effects similar to increasing pressure — lateral temperature changes are similar to vertical pressure changes. The curve labeled $\alpha\Delta T$ is the approximate effect of thermal expansion alone on density. The bar labeled 800°C shows the expected change in temperature across a subducted slab and is approximately half the maximum expected lateral temperature changes in the mantle. Note that a temperature change of 800°C placed anywhere in the field of temperatures expected in the mantle will cross one, two or even three phase boundaries, each of which contributes a density change in addition to the $\alpha\Delta T$ term from thermal expansion. Changes in elastic properties are associated with these phase changes.

Figure 16-7 shows the approximate zero-pressure room-temperature density for the CMAS system with a low-pressure mineralogy appropriate for garnet peridotite with olivine > orthopyroxene > clinopyroxene ≈ garnet. Note that the low-temperature phase assemblages are denser than high-temperature assemblages (normal mantle) until about 210 kbar and that the differences are particularly pronounced between about 300 and 550 km. The density change associated with a temperature change of 800 K ranges from 7 to 17 percent in the temperature interval 1000 to 2300 K at pressures of 180 and 200 kbar. This includes thermal expansion and isobaric phase changes. Thermal expansion alone gives 2 to 3 percent. Note that the density anomaly associated with the slab is far from constant with depth. Furthermore, the density anomaly of a slab with respect to the adjacent mantle is quite different from the den-

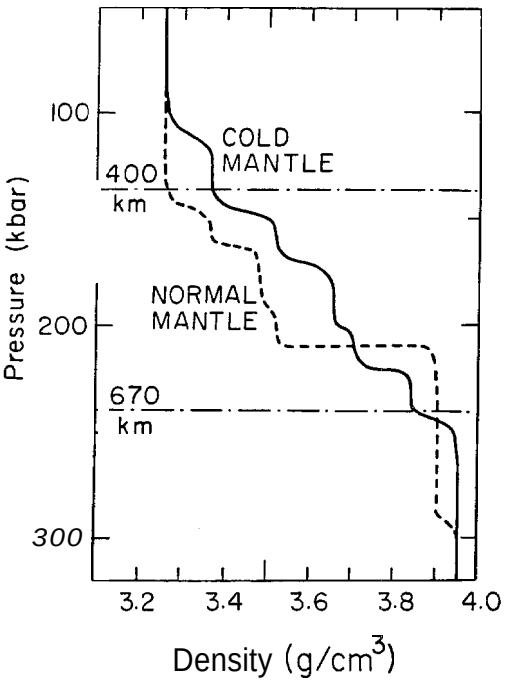

FIGURE 16-7
Zero-pressure room-temperature density of FeO-free peridotite (olivine > orthopyroxene > clinopyroxene ≈ garnet) using mineral assemblages appropriate for the temperatures in warm ("normal") mantle and slab ("cold") mantle and the phase relations of Figure 16-5 (after Anderson, 1987b).

sity contrast between the surface plate and the underlying mantle, as estimated from the bathymetry-age relation for oceanic plates.

The important phase changes in the mantle mostly have Clapeyron slopes that correspond to depth variations of 30–100 km per 1000°C. The widths of the phase changes, at constant temperature when solid-solid effects are taken into account, are, for example, 40 kbar for complete transformation of a-olivine to y-spinel, about 10 kbar for $\alpha-\beta$ and 40 kbar for $\beta-\gamma$. The comparable changes, at constant pressure, occur over a temperature interval of 300°C, which is less than half the temperature contrast across a subducting slab.

By use of Figure 16-8 or 16-5 we see that several phase boundaries are crossed in going, at constant pressure, from normal mantle temperatures to colder temperatures. For example, near 150 kbar, olivine and pyroxenes are stable at high temperature, β-spinel, majorite and clinopyroxene are stable at lower temperatures and $\beta \pm$ stishovite $\pm$ clinopyroxene is the stable assemblage at cold temperature. At 230 kbar calcium-rich perovskite, $MgSiO_3$-perovskite and magnesiowiistite is the normal assemblage, and ilmenite replaces $MgSiO_3$-perovskite at cold temperature. Garnet is stable over a very large pressure and temperature range. This is important since large amounts of garnet will decrease both the radial and lateral variations in physical properties.

The question of whether eclogite becomes less dense than peridotite at pressures near the base of the transition region and top of the lower mantle has been controversial. One side has maintained that eclogite becomes less dense than peridotite at the base of the transition region and is less dense than the top of the lower mantle (Anderson, 1979a,b; Anderson and Bass, 1984). The primary reason is the large stability interval of garnet. Ringwood and coworkers have maintained until recently that eclogite is denser than peridotite at all pressures. Very recently they were able to extend the pressure range of their experiments (Irifune and others, 1986), and they show that the densities of eclogite of MORB composition and peridotite do indeed intersect at high pressure. Quartz-free eclogites will actually be less dense than they calculate since MORB-eclogite has a large SiO_2-stishovite component. The crustal component of the slab, even if it survives subduction to 650 km, does not control its own destiny. It is the integrated density of the slab, intrinsic density contrast across the 650-km discontinuity and pressure-temperature locations of phase boundaries in the slab and lower mantle that determine whether slabs will be able to sink into the lower mantle. In a chemically layered mantle the "650-km" discontinuity will be depressed by the subducted slab and therefore, in this sense, the upper mantle protrudes into the lower mantle or, more precisely, protrudes below the depth usually assigned to the upper mantle–lower mantle boundary. Whether it can protrude deeply enough to be entrained in lower-mantle flow

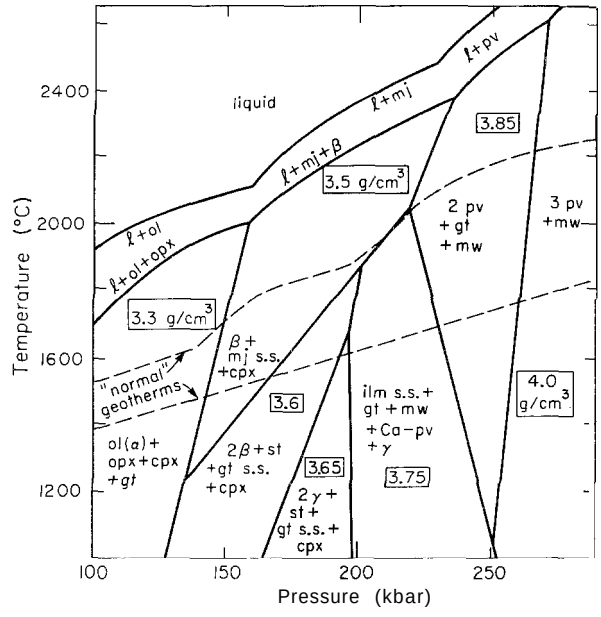

FIGURE 16-8
Tentative phase relations in the system $MgO\text{-}SiO_2\text{-}CaO\text{-}Al_2O_3$ with an ol > opx > cpx ≈ gt mineralogy at low pressure, based on a synthesis of a variety of subsolidus and melting experiments on peridotites. The geotherms bracket most estimates of temperatures in "normal" or average mantle. Warmer parts of the mantle may be near the solidus; the interiors of slabs may be 800°C colder. The phase diagram is based on incomplete and sometimes inconsistent reconnaissance experiments and must be taken as provisional until systematic and reversed experiments are performed. Based on experiments and interpretations by Kato and Kumazawa (1985, 1986), Akaogi and Akimoto (1977), Ohtani and others (1986a,b), Kanzaki (1986), Ito and Takahashi (1986), Yamada and Takahashi (1984), Irifune and others (1986), and Sawamoto (1986). "2β" and "2γ" mean that both Mg_2SiO_4 and $MgSiO_3$ have transformed to a spinel assemblage (Anderson, 1987; after Anderson, 1987b).

or to overcome the negative Clapeyron slope or whether, even in this case, it can become denser than the lower mantle, are questions that have yet to be completely addressed. The seismic problem of determining whether slabs are continuous across the upper-lower mantle boundary (the depressed "650-km discontinuity") is complicated by the likely presence of a detached thermal boundary layer at the top of the lower mantle under such conditions. This would be dense and fast and would be hard to distinguish from a penetrating slab. In this regard, the complete lack of seismicity below about 690 km and the apparent crumpling of the slab near this depth are significant (Giardini and Woodhouse, 1984).

In peridotite the density in the lower part of the transition region (Figure 16-8 and 16-9) is dominated by β-spinel (ρ, = 3.47 g/cm³) or y-spinel (3.56 g/cm³) and majorite (3.52 g/cm³) or ilmenite (3.82 g/cm³). In eclogite the mineralogy is garnet (3.56 g/cm³), calcium-perovskite

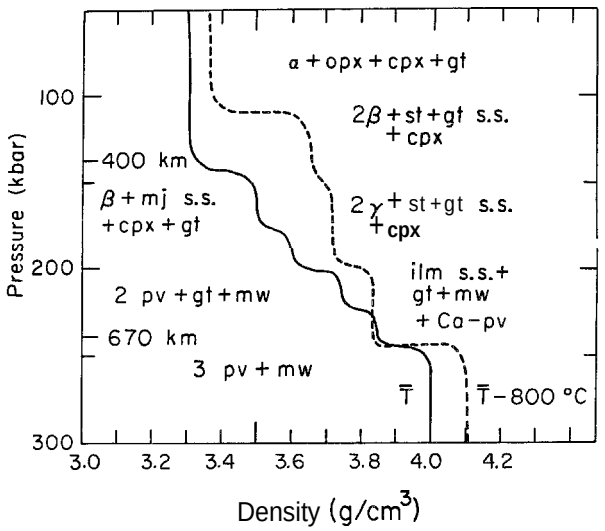

FIGURE **16-9**
Zero-pressure density for peridotite at two temperatures (the mean of the "normal" geotherms and a temperature 800°C colder). Phase changes and thermal expansion are included. The density differences would be different for an eclogitic mantle or for a slab that differs in chemistry from the surrounding mantle. Abbreviations are α(olivine), opx (orthopyroxene), cpx (clinopyroxene), gt (garnet), gt s.s. (garnet plus majorite, mj), st (stishovite), ilm s.s. ($MgSiO_3$ ilmenite + gt-ilmenite), mw (magnesiowiistite) (Anderson, 1987b).

(−4.1 g/cm³) and possibly Al_2O_3 (3.99 g/cm³) and MgO (3.58 g/cm³). An eclogitic slab will therefore have a density between about 4 g/cm³ (calcium-perovskite + Al_2O_3) and 3.56 g/cm³ (garnet), which is less than the uncompressed density of the lower mantle (Butler and Anderson, 1978). Therefore, neither harzburgite nor eclogite have densities high enough to sink into the lower mantle, and we expect a barrier to slab penetration, and thickening and lateral flow of subducted material, at the base of the transition region. A large jump in viscosity near 650 km (Hager, 1984) also provides a barrier to slab penetration, but in a chemically homogeneous mantle, upper mantle material eventually circulates into the lower mantle. In either case, the slab does not slide easily into the lower mantle as implied in the thermal models of Creager and Jordan (1984, 1986). The high density of the slab, relative to adjacent mantle, contributes to the geoid and seismic-velocity anomalies associated with subduction zones and, in general, will increase the dips of Wadati-Benioff zones compared to strictly thermal models of the slab.

There is little information on the variation in depth of the 650-km discontinuity, but it is unlikely to vary by more than 100 km from its mean depth. A determination of the actual depth of the discontinuity under slabs will constrain the integrated density contrast of the slab and the nature of the boundary. An interesting question is whether the average composition of the slab is the same as the surrounding mantle, as assumed in most discussions. An eclogitic slab, for example, sinking through a peridotitic mantle would cause a smaller depression of a chemical interface at 650 km than a peridotitic slab.

Velocity anomalies associated with slabs are about +4 percent at 50 km, +10 percent at 100 km, +3 to 10 percent from 200 to 300 km, +4 to 7 percent at 400 km, +2 to 5 percent at 450 km, +4 to 5 percent at 500 km, +12 ± 4 percent at 620 km, +9 ± 3 percent at 650 km and +8 ± 2 percent between 580 and 660 km (Fitch, 1975; Hirahara, 1977; Huppert and Frohlich, 1981; Hirahara and Ishikawa, 1984; Engdahl and Gubbins, 1988). A AT of 800°C and a velocity contrast of 6 percent gives $\partial V_p/\partial T = -6.4 \times 10^{-4}$km/s °C. A 12 percent velocity contrast would double this figure. Allowing for the averaging of seismic waves across the temperature gradient would also raise the implied temperature derivatives. The values of $\partial V_p/\partial T$ for MgO, Al_2O_3, olivine, spinel and garnets fall in the range -3 to -5.2×10^{-4}km/s °C, which are less than the values implied by the seismic data for a purely thermal effect. Furthermore, temperature derivatives are expected to decrease rapidly with pressure. Changes in phase or composition from "normal" mantle are therefore implied since purely thermal effects are small. Thus, both the phase equilibria calculations and the seismic data support the presence of isobaric phase changes across the slab.

Seismic velocity differences between low-pressure assemblages involving olivine and orthopyroxene and high-pressure assemblages involving β- and y-spinel and majorite or stishovite are of the order of 10 percent, and these are expected to be elevated in the cold slab by 100 to 150 km. Therefore, the slab velocity anomaly should be particularly large between about 300 and 400 km. The observed velocity contrast is smaller than the temperature-plus-phase change effect in an olivine-orthopyroxene mantle, suggesting that there is about 50 percent of "inert" component in the slab, material that does not transform over this pressure interval. Garnet is stable to about 600 km, and clinopyroxene (diopside ± jadeite) is stable to about 500 km. The implication is that the slab is garnet-clinopyroxene-rich relative to most garnet peridotites, which are samples from the shallow mantle. The possibility that the average composition of the slab is not the same as the average composition of the upper mantle complicates the interpretation of slab anomalies and the calculation of the depression of chemical discontinuities by subducted slabs.

The observed slab anomalies are comparable to and greater than the velocity jumps associated with mantle discontinuities. This strongly suggests that lateral velocity changes in the mantle, particularly near subducted slabs, involve isobaric phase changes as well as temperature variations. The velocity jump at the 400-km discontinuity is about 4–5 percent. This also suggests that garnet and clinopyroxene are important components of the mantle near

400 km; otherwise the velocity jump would be much greater.

The high gradient in seismic velocity between about 400 and 600 km depth implies a gradual phase change or series of phase changes occurring over this depth interval. The candidate transformations are majorite to β + stishovite, β to y, γ + stishovite to ilmenite, and clinopyroxene to garnet or perovskite. The increase of the slab seismic anomaly below about 500 km is consistent with major isobaric phase changes occurring below this depth.

The measured or estimated compressional velocities of the important phases of upper-mantle minerals are shown in Figure 16-10. Also shown are the estimated velocities for pesidotite at two temperatures, taking into account the different stable phase assemblages. The major differences occur between about 130 and 225 kbar. The heavy lines show the approximate stability pressure range for the various phases. Garnet and clinopyroxene represent less than 20 percent of the chosen peridotite composition. Since these minerals are stable to about 260 and 200 kbar, respectively, the effect of density and velocity changes associated with phase changes as both a function of temperature and pressure will be lower for less olivine and orthopyroxene-rich mantle. The deformation of the 650-km discontinuity, if this is a chemical boundary, will also be less.

Creager and Jordan (1986) used intermediate-depth earthquakes (149 to 256 km) to calibrate the effect of the underlying slab on travel times of deeper focus earthquakes. It is clear from Figure 16-10 that the velocity anomaly below intermediate-depth events is not similar to that expected below the deeper events (585 and 624 km) used in their analysis. (These depths correspond to pressures of 200–220 kbar.) Not only are the average velocity contrasts different, but the anisotropies of the stable phase assemblages are also quite different. Any degree of preferred orientation in the slab and the adjacent mantle will affect the differential travel times of rays leaving the source in different directions. A more direct determination of velocity anomalies in the vicinity of intermediate-depth earthquakes is about 5–6 percent (Engdahl and Gubbins, 1988). The velocity anomaly in the vicinity of deep-focus earthquakes appears to be much greater, in agreement with the above expectations. There is a direct trade-off between the magnitude of the velocity contrast in the vicinity of deep-focus earthquakes and normal mantle, and the depth extent of the slab beneath these earthquakes in the interpretation of residual sphere anomalies. A 10 percent velocity contrast and a slab extending only 100 km beneath the source gives a travel-time anomaly of 1.5 s for rays sweeping out of a cone of 45° to the plane of the slab. This is about the range of travel-time anomalies observed. The smaller velocity anomalies assumed by Creager and Jordan require much deeper slab penetration. Creager and Jordan assumed a contrast of 10 percent in their 1984 paper, but their calculations are obviously in error since their deep slab model predicts approximately 8-s anomalies, much greater than observed. Their results, when corrected, are consistent with a short slab.

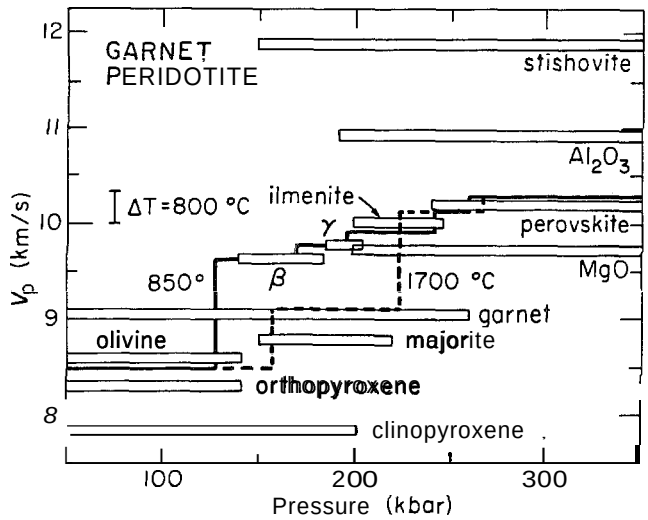

FIGURE **16-10**
Compressional velocities, at standard conditions, and stability fields of mantle minerals. The approximate velocity of garnet peridotite, at standard conditions ($P = 0$, $T \approx 20°C$) for phases stable at two temperatures (850°C, 1700°C) is also shown. The small bar gives the approximate change in V_p for a 800°C change in temperature ($\partial V_p/\partial T = -4.1 \times 10^{-4}$ km/s°C).

The small bar in Figure 16-10 shows a typical change of V_p for an 800°C temperature change, assuming no phase changes. Note that the effect of the more important phase changes is to double or triple the effect of temperature. The largest effects occur between about 130 and 230 kilobars, the pressure range of deep-focus earthquakes. Note that clinopyroxene and garnet, minor constituents of peridotite and pyrolite but major components of eclogite and piclogite (Bass and Anderson, 1984), have the largest stability fields of low-pressure minerals. The presence of clinopyroxene and garnet reduces the size of the phase-change effects in the upper part of the transition region, particularly near 400 km. The smallness of the velocity jump near 400 km, both radially and laterally, indicates the presence of substantial amounts of a "neutral" component—garnet and clinopyroxene—near this depth. These are the dominant minerals in eclogite. On the other hand, eclogite experiences major transformations and velocity increases between 200 and 250 kbar, a pressure range pertinent to the velocity anomaly near deep-focus earthquakes.

General References

Akaogi, M. and S. Akimoto (1977) Pyroxene-garnet solid solution equilibrium, Phys. *Earth* Planet. *Int.*, *15*, 90–106.

Akaogi, M., A. Navrotsky, T. Yagi and S. Akimoto (1986) Pyrox-

ene-garnet transformation, U.S.-Japan Seminar, Jan. 13–16, 1986, Program with Abstracts, 46.

Akimoto, S. (1972) The system MgO-FeO-SiO_2 at high pressure and temperature, *Tectonophysics, 13,* 161–187.

Anderson, D. L. (1967) Latest information from seismic observations. In *The Earth's Mantle* (T. F. Gaskell, ed.), 355–420, Academic Press, New York.

Anderson, D. L. (1981) A global geochemical model for the evolution of the mantle. In *Evolution of the Earth* (R. J. O'Connell, ed.), 6–18, American Geophysical Union, Washington, D.C.

Anderson, D. L. (1982) Chemical composition of the mantle, *Jour. Ceophys. Res., 88,* B41–B52.

Anderson, D. L. (1982) The chemical composition and evolution of the mantle. In *High-pressure Research in Geophysics* (S. Akimoto and M. H. Manghnani, eds.), 301–318, D. Reidel, Dordrecht.

Anderson, D. L. (1987a) A seismic equation of state II, *Phys. Earth Planet. Int.*

Anderson, D. L. and J. Bass (1986) Transition region of the Earth's upper mantle, *Nature, 320,* 321–328.

Bloss, F. D. (1971) *Crystallography and Crystal Chemistry,* Holt Rinehart and Winston, New York, 545 pp.

Frohlich, C. and M. Barazangi (1980) A regional study of mantle velocity variations beneath eastern Australia and the southwestern Pacific using short-period recordings of P, S, PcP, ScP and ScS waves produced by Tonga deep earthquakes, *Phys. Earth Planet. Inter., 21,* 1–14.

Fyfe, W. S. (1964) *Geochemistry of Solids,* McGraw-Hill, New York, 199 pp.

Hager, B. H. and R. Clayton (1987) Constraints on the structure of mantle convection using seismic observations, flow models, and the geoid (in press).

Ito, E. and H. Yamada (1982) Stability relations of silicate spinels, ilmenite and perovskites. In *High-pressure Research in Geophysics* (S. Akimoto and M. Manghnani, eds.), 405–419, D. Reidel, Dordrecht.

Ito, E. and E. Takahashi (1986) Ultra high-pressure phase transformations and the constitution of the deep mantle, in *High-Pressure Research in Mineral Physics* (ed. M. Manghnani and Y. Syono), *Geophys.* Monograph 34, Amerian Ceophys. Union, Washington, D.C., 486 pp.

Jeanloz, R. and E. Knittle (1986) Reduction of mantle and core properties to a standard state by adiabatic decompression. In *Chemistry and Physics of the Terrestrial Planets* (S. K. Saxena, ed.), 275–305, Springer-Verlag, New York.

Kanzaki, M. (1986) Ultrahigh-pressure phase relations in the system $MgSiO_3$-$Mg_3Al_2Si_3O_{12}$, *Phys. Earth Planet. Int.*

Kato, T. and M. Kumazawa (1985) Garnet phase of $MgSiO_3$ filling the pyroxene-ilmenite gap at very high temperature, *Nature, 316,* 803–805.

Kato, T. and M. Kumazawa (1986) Melting and phase relations in the Mg_2SiO_4–$MgSiO_3$ system at 20 GPa under hydrous conditions, *J. Geophys. Res., 91,* 9351–9355.

Kuskov, O. L. and R. Galimzyanov (1986) Thermodynamics of stable mineral assemblages of the mantle transition zone. In *Chemistry and Physics of the Terrestrial Planets* (S. K. Saxena, ed.) 310–361, Springer-Verlag, New York.

Liu, L. (1974) Silicate perovskite from phase transformation of pyrope garnet, *Geophys. Res. Lett., 1,* 277–280.

Ohtani, E. (1983) Melting temperature distribution and fractionation in the lower mantle, *Phys. Earth Planet. Inter., 33,* 12–25.

Ohtani, E. (1985) The primordial terrestrial magma ocean and its implications for stratification of the mantle, *Phys. Earth Planet. Inter., 38,* 70–80.

Ohtani, E., T. Kato and H. Sawamoto (1986a) Melting of a model chondritic mantle to 20 GPa, *Nature, 322,* 352–354.

Ohtani, E., C. T. Herzberg and T. Kato (1986b) Majorite stability, *Earth Planet. Sci. Lett.*

Pauling, L. C. (1979) *J. Am. Chem. Soc., 51,* 1010.

Ringwood, A. and A. Major (1970) The system Mg_2SiO_4–Fe_2SiO_4 at high pressures and temperatures, *Phys. Earth Planet. Int., 3,* 89–108.

Ringwood, A. E. (1975) *Composition and Petrology of the Earth's Mantle,* McGraw-Hill, New York, 618 pp.

Ringwood, A. E. (1982) Phase transformations and differentiation in subducting lithosphere, *Jour. Geol., 90,* 611–643.

Ringwood, A. E. and A. Major (1971) Synthesis of majorite and other high pressure garnets and perovskites, *Earth Planet. Sci. Lett., 12,* 411–418.

Sawamoto, H. (1986) Phase equilibrium of $MgSiO_3$ under high pressure and high temperature, U.S.–Japan Seminar, Jan. 13–16, 1986, Program with Abstracts, 50–51.

Yamada, H. and E. Takahashi (1984) Subsolidus phase relations between coexisting garnet and two pyroxenes at 50 to 100 kb in the system CaO-MgO-Al_2O_3-SiO_2. In *Kimberlites II: The Mantle and Crust Relationships* (J. Kornprobst, ed.), 247–255, Elsevier, Amsterdam.

References

Akaogi, M., N. Ross, P. McMillen and A. Navrotsky (1984) The Mg_2SiO_4 polymorphs; thermodynamic properties from oxide melt solution calorimetry, phase relations, and models of lattice vibrations, *Am. Mineral., 69,* 499–512.

Anderson, D. L. (1979a) The upper mantle transition region: Eclogite? *Geophys. Res. Lett., 6,* 433–436.

Anderson, D. L. (1979b) Chemical stratification of the mantle, *Jour. Geophys. Res., 84,* 6297–6298.

Anderson, D. L. (1987b) Thermally induced phase changes, lateral heterogeneity of the mantle, continental roots, and deep slab anomalies, J. *Geophys. Res., 92,* 13,968–13,980.

Anderson, D. L. and J. D. Bass (1984) Mineralogy and composition of the upper mantle, *Geophys. Res. Lett., 11,* 637–640.

Butler, R. and D. L. Anderson (1978) Equation of state fits to the lower mantle and outer core, *Phys. Earth Planet. Int., 17,* 147–162.

Creager, K. C. and T. H. Jordan (1984) Slab penetration into the lower mantle, J. *Geophys. Res., 89,* 3031–3049.

Creager, K. C. and T. H. Jordan (1986) Slab penetration into the lower mantle beneath the Mariana and other island arcs of the northwest Pacific, J. *Geophys. Res., 3,* 3573–3580.

Engdahl, E. R. and D. Gubbins (1988) Simultaneous travel-time inversion for earthquake location and subduction zone structure in the central Aleutian Islands, J. *Geophys. Res., 92,* 13,855.

Fitch, T. J. (1975) Compressional velocity in source regions of deep earthquakes, *Earth Planet. Sci. Lett., 26,* 156–166.

Giardini, D. and J. H. Woodhouse (1984) Deep seismicity and modes of deformation in Tonga subduction zone, *Nature, 307,* 505–509.

Hager, B. H. (1984) Subducted slabs and the geoid; constraints on mantle rheology and flow, J. *Geophys. Res., 89,* 6003–6015.

Hirahara, K. (1977) A large-scale three-dimensional seismic structure under the Japan islands and the Sea of Japan, J. *Phys. Earth, 25,* 393–417.

Hirahara, K. and Y. Ishikawa (1984) Travel time inversion for three-dimensional P-wave velocity anisotropy, J. *Phys. Earth, 32,* 197–218.

Huppert, L. and C. Frohlich (1981) The P velocity within the Tonga Benioff zone, J. *Geophys. Res., 86,* 3771–3782.

Irifune, *T.* and A. E. Ringwood (1986) Phase transformations in primitive MORB and pyrolite compositions to 25 GPa and some geophysical implications, High-pressure Research in Mineral Physics, Proceedings of the U.S.-Japan Seminar (ed. M. Manghnani and Y. Syono), *Geophys.* Monograph 39, American Geophysical Union, Washington, D.C., 486 pp.

Irifune, T., T. Sekine, A. E. Ringwood and W. O. Hibberson (1986) The eclogite-garnet transformation at high pressure and some geophysical implications, *Earth Planet. Sci. Lett., 77,* 245–256.

Ito, E. and A. Navrotsky (1985) $MgSiO_3$ ilmenite; calorimetry, phase equilibria, and decomposition at atmospheric pressure, *Am. Mineral.,* 70, 1020–1026.

Navrotsky, A., F. S. Pintchovski and S. Akimoto (1979) Calorimetric study of the stability of high pressure phases in the systems CoO-SiO_2 and "FeO"-SiO_2, and calculation of phase diagrams in MgO-SiO_2 systems, *Phys. Earth Planet. Int., 19,* 275–292.

Richards, M. A. and B. H. Hager (1984) Geoid anomalies in a dynamic Earth, J. *Geophys. Res., 89,* 5987–6002.

Watanabe, H. (1982) Thermochemical properties of synthetic high-pressure compounds relevant to the Earth's mantle. In *High-pressure Research in Geophysics (S.* Akimoto and M. Manghnani, eds.), 441–464, Elsevier, Amsterdam.